AIP | Physics of Plasmas

The relation between reconnected flux, the parallel electric field, and the reconnection rate in a three-dimensional kinetic simulation of magnetic reconnection

D. E. Wendel, D. K. Olson, M. Hesse, N. Aunai, M. Kuznetsova, H. Karimabadi, W. Daughton, and M. L. Adrian

Citation: Physics of Plasmas (1994-present) **20**, 122105 (2013); doi: 10.1063/1.4833675
View online: http://dx.doi.org/10.1063/1.4833675
View Table of Contents: http://scitation.aip.org/content/aip/journal/pop/20/12?ver=pdfcov
Published by the AIP Publishing

Articles you may be interested in

Experimental observation of 3-D, impulsive reconnection events in a laboratory plasma
Phys. Plasmas **21**, 012109 (2014); 10.1063/1.4862039

Magnetohydrodynamic study for three-dimensional instability of the Petschek type magnetic reconnection
Phys. Plasmas **20**, 122118 (2013); 10.1063/1.4846857

Kinetic simulations of the structures of magnetic island in multiple X line guide field reconnection
Phys. Plasmas **19**, 042111 (2012); 10.1063/1.4704799

Gyrokinetic simulations of magnetic reconnection
Phys. Plasmas **18**, 112102 (2011); 10.1063/1.3656965

Magnetohydrodynamic study of three-dimensional instability of the spontaneous fast magnetic reconnection
Phys. Plasmas **16**, 052903 (2009); 10.1063/1.3095562

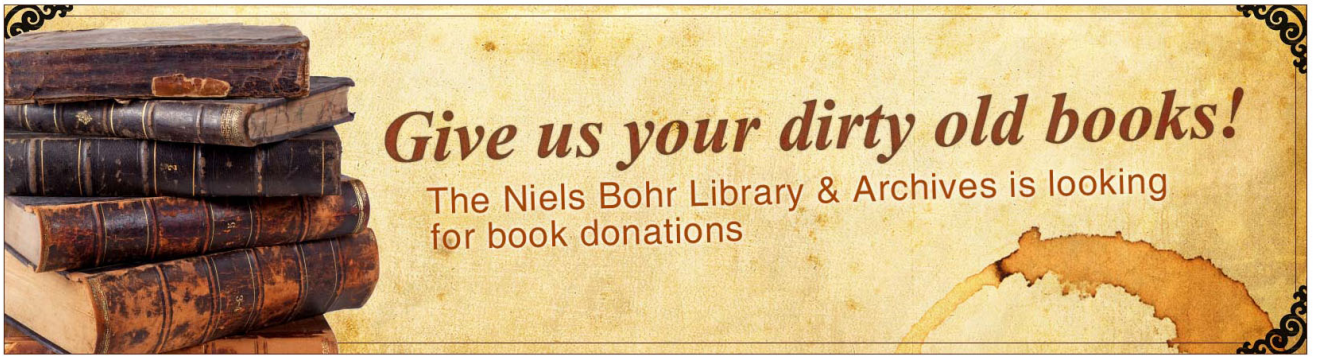

This article is copyrighted as indicated in the article. Reuse of AIP content is subject to the terms at: http://scitation.aip.org/termsconditions. Downloaded to IP: 128.154.130.33 On: Mon, 23 Jun 2014 20:00:33

The relation between reconnected flux, the parallel electric field, and the reconnection rate in a three-dimensional kinetic simulation of magnetic reconnection

D. E. Wendel,[1] D. K. Olson,[1] M. Hesse,[1] N. Aunai,[2] M. Kuznetsova,[1] H. Karimabadi,[3,4] W. Daughton,[5] and M. L. Adrian[1]
[1]*NASA Goddard Space Flight Center, Greenbelt, Maryland 20771, USA*
[2]*Institute for Research in Astrophysics and Planetology, University Paul Sabatier, Toulouse, France*
[3]*SciberQuest, Inc., Del Mar, California 92014, USA*
[4]*Department of Computer and Electrical Engineering, University of California, San Diego, La Jolla, California 92093, USA*
[5]*Los Alamos National Laboratory, Los Alamos, New Mexico 87545, USA*

(Received 18 September 2013; accepted 4 November 2013; published online 11 December 2013)

We investigate the distribution of parallel electric fields and their relationship to the location and rate of magnetic reconnection in a large particle-in-cell simulation of 3D turbulent magnetic reconnection with open boundary conditions. The simulation's guide field geometry inhibits the formation of simple topological features such as null points. Therefore, we derive the location of potential changes in magnetic connectivity by finding the field lines that experience a large relative change between their endpoints, i.e., the quasi-separatrix layer. We find a good correspondence between the locus of changes in magnetic connectivity or the quasi-separatrix layer and the map of large gradients in the integrated parallel electric field (or quasi-potential). Furthermore, we investigate the distribution of the parallel electric field along the reconnecting field lines. We find the reconnection rate is controlled by only the low-amplitude, zeroth and first–order trends in the parallel electric field while the contribution from fluctuations of the parallel electric field, such as electron holes, is negligible. The results impact the determination of reconnection sites and reconnection rates in models and *in situ* spacecraft observations of 3D turbulent reconnection. It is difficult through direct observation to isolate the loci of the reconnection parallel electric field amidst the large amplitude fluctuations. However, we demonstrate that a positive slope of the running sum of the parallel electric field along the field line as a function of field line length indicates where reconnection is occurring along the field line. © *2013 AIP Publishing LLC*. [http://dx.doi.org/10.1063/1.4833675]

I. INTRODUCTION

Magnetic reconnection is a universal phenomenon in magnetized plasmas that converts magnetic field energy into kinetic particle energy. The theory of magnetic reconnection and its redistribution of magnetic flux changes dramatically when it incorporates 3D spatial dependence of fields and particles. While the separatrices that govern the location and rate of reconnection are lines at null points in 2D, at 3D null points they are surfaces called fan planes,[1–3] for example. In 2D, reconnection is readily defined as the discontinuous mapping of field lines and flow of plasma across the separatrices, and the reconnection rate is defined as the out-of-plane electric field at the x-point.[4–6] In 3D reconnection with null points, reconnection may entail flux across the fan plane. The case of 3D reconnection in an ambient background magnetic field, however, inhibits the formation of null points and their associated separatrices and separators and therefore requires a more general definition for the occurrence and rate of reconnection. In this case, the reconnection rate is defined as the maximum of the integral of the parallel electric field along the field lines that thread the diffusion region, or the quasi-potential, while a necessary and sufficient condition for its occurrence is a spatial gradient of the quasi-potential.[7–9] From a topological point of view, flux is transported across layers of neighboring field lines whose endpoint locations move rapidly and differ dramatically but continuously, rather than across well-defined separatrix surfaces whose endpoint locations differ discontinuously.[10,11] The increased complexity of the topology and the particle behavior in general 3D reconnection presents a challenge to identifying the location and rate of magnetic reconnection in observations and simulations, which may be further complicated by the development of turbulence.[12–16]

Here we present results that identify the location and rate of reconnection in a 3D kinetic particle-in-cell simulation and show that the predictions of both the quasi-potential and topological pictures mentioned above coincide. The VPIC code,[17,18] executed on the Cray supercomputer Kraken, simulates solutions to the set of Vlasov-Maxwell equations over a domain of $70d_i \times 35d_i \times 70d_i$, where $d_i = c/\omega_{pi}$ is the ion skin depth, with a mass ratio $m_i/m_e = 100$ and a grid resolution of approximately 0.34 d_e, where d_e is the electron skin depth. In practice, boundary conditions are open in x and z, and periodic along y, the direction of the initial current layer. The simulation thus represents a large open system over a large range of scales. A weak (4%) perturbation (consistent with the boundary conditions) is imposed on an initial Harris equilibrium with a half-thickness of an ion skin depth. A primary

 © 2013 AIP Publishing LLC

This article is copyrighted as indicated in the article. Reuse of AIP content is subject to the terms at: http://scitation.aip.org/termsconditions. Downloaded to IP: 128.154.130.33 On: Mon, 23 Jun 2014 20:00:33

tearing instability leads to the generation of oblique flux ropes. In addition, a secondary tearing instability of elongated electron current layers lead to the formation of secondary flux ropes. Flux ropes generated at these scales quickly grow well above ion scales and overlap, leading to the interaction of highly anisotropic and inhomogeneous structures across multiple scales, a stochastic magnetic field, and turbulence.[19] Turbulence continues to be self-generated within the reconnection layer.[13,16] For this study, we analyze the volume over one time step for the same run discussed in depth by Daughton *et al.*[13] Reconnection is well underway, at $t\Omega_{ci} = 98$, where Ω_{ci} is the ion cyclotron frequency. Other parameters of the system are $T_i = T_e$, $B_y = B_{x0}$, and $n_{cell} = 120$, where T_i and T_e are the ion and electron temperature, B_y is the guide field, B_{x0} is the initial reconnecting field, and n_{cell} is the number of particles per cell per species.

We first pursue a topological approach by determining the quasi-separatrix layer where it is predicted reconnection may occur if there is also a parallel electric field.[10,11] Even if separatrices and separators do occur in a guide field simulation, they will be very difficult to find and are not relevant to the analysis we propose here. By integrating the parallel electric field along field lines, we then produce a 2D map of the quasi-potential as a function of the Euler coordinates at the starting y-plane of the integration. The theory of general magnetic reconnection predicts that reconnection occurs on those field lines that have a gradient with respect to the Euler coordinates of the integral of the parallel electric field while the maximum value of the integral of the parallel electric field gives the reconnection rate.[7–9] We then compare the predictions of both analyses. The combination of these two analyses indicates which field lines in the simulation are reconnecting. To determine where it is occurring along the length of a given field line, however, we calculate the partial, running sum of the quasi-potential, i.e., the parallel electric field summed up to a given position along the field line as a function of position along the field line. This approach serves to smooth over the large amplitude fluctuations in the parallel electric field and thus reveals where along the field line the parallel electric field contributes to the reconnection rate. We also examine the relative contributions of DC and low-order components and of higher-order fluctuations of the parallel electric field to the reconnection rate. Our determination of the reconnection rate from the parallel electric field differs from the analysis in Liu *et al.*,[20] which finds the average parallel electric field over a selected region. Here we make a spatial map of the quasi-potential, for comparison against the quasi-separatrix layer, and find the reconnection rate from an estimate of the maximum value of the quasi-potential. We begin our discussion with a brief description of the theory of general magnetic reconnection and of reconnection on quasi-separatrix layers. We then proceed to discuss our implementation of these ideas to the volume of VPIC simulation data and analyze and compare the results. Finally, we investigate the characteristics of the parallel electric field and the distribution of the reconnection rate along field lines.

II. THEORY OF GENERAL MAGNETIC RECONNECTION

Hesse and Schindler[7] and Schindler *et al.*[9] show that separatrices are not defined in the most general case of 3D reconnection with a non-vanishing magnetic field. Therefore the classic 2D identification of reconnection with the intersection of separatrix surfaces is no longer applicable in general. Working in terms of Euler potentials, they propose a more general definition of reconnection and the reconnection rate that encompasses those instances. Rather than relying on topological definitions, they derive the necessary and sufficient condition for reconnection from a measure of the change in magnetic flux.

In the vicinity of a region of interest, the magnetic field and the magnetic vector potential $\mathbf{A}$ may be expressed in terms of Euler potentials $\alpha(x,y,z)$ and $\beta(x,y,z)$ as

$$\begin{aligned} \mathbf{B} &= \nabla\alpha \times \nabla\beta, \\ \mathbf{A} &= \alpha\nabla\beta. \end{aligned} \tag{1}$$

Though they are not unique, as any α and β that satisfy the expressions for $\mathbf{B}$ and $\mathbf{A}$ in Eq. (1) are allowed, each α and β uniquely define a field line if the domain through which $\mathbf{B}$ passes is simply connected.[22] They are also the flux coordinates such that

$$\Phi = \int d\alpha d\beta, \tag{2}$$

where Φ is the magnetic flux.[22] One may then define a quasi-potential Ψ and an electric field $\mathbf{E}$ in terms of static and time-dependent contributions as

$$\begin{aligned} \Psi &= \varphi + \frac{\alpha}{c}\frac{\partial\beta}{\partial t}, \\ \mathbf{E} &= -\frac{1}{c}\left[\frac{\partial\alpha}{\partial t}\nabla\beta + \frac{\partial\beta}{\partial t}\nabla\alpha\right] - \nabla\Psi, \end{aligned} \tag{3}$$

where φ is the static potential and c is the speed of light. Here we have expressed quantities in cgs units for consistency with later calculations. Inserting these terms into the nonideal Ohm's law, the authors derive an expression for the time rate of change for α and β and for the dependence of Ψ on the field line length s.[7,8]

To derive the conditions for reconnection, Hesse and Schindler[7] find a general expression for the change in magnetic flux across a non-ideal region. If a localized non-ideal region produces a parallel potential drop along a field line, then the quasi-potential differs on either side of the non-ideal region by

$$\Xi = \Psi_2 - \Psi_1 = -\int_{\alpha,\beta} E_{||} dl, \tag{4}$$

where $E_{||}$ is the parallel electric field. A difference in the time rate of change of the flux coordinates α and β on either side of the non-ideal region, i.e., $d\alpha/dt|_1 \neq d\alpha/dt|_2$ and $d\beta/dt|_1 \neq d\beta/dt|_2$, reveals that connections between field line elements threading the non-ideal region have changed in

This article is copyrighted as indicated in the article. Reuse of AIP content is subject to the terms at: http://scitation.aip.org/termsconditions. Downloaded to IP: 128.154.130.33 On: Mon, 23 Jun 2014 20:00:33

time. Hesse and Schindler[7] and Hesse *et al.*[8] show that the difference in evolution of the flux coordinates on either side equates to

$$\left.\frac{d\alpha}{dt}\right|_2 - \left.\frac{d\alpha}{dt}\right|_1 = -\frac{\partial \Xi}{\partial \beta}, \qquad \left.\frac{d\beta}{dt}\right|_2 - \left.\frac{d\beta}{dt}\right|_1 = \frac{\partial \Xi}{\partial \alpha}. \tag{5}$$

They therefore deduce that a necessary and sufficient condition for reconnection is

$$\nabla_{\alpha,\beta}\Xi(\alpha,\beta) \neq 0. \tag{6}$$

They show, furthermore, that the Hamiltonian form of the expressions in Eq. (5) produces changes of Ξ in α-β space, and therefore new field line connections, in closed loops. It is not Ξ *per se,* but rather the gradients of Ξ across field lines that form the necessary and sufficient prerequisite for reconnection. Hesse *et al.*[8] also show that the rate at which flux is reconnected across an entire flux surface is given by $\max(\int E_{||} dl) = -\max(\Xi)$.

III. THEORY OF MAGNETIC FLIPPING ON QUASI-SEPARATRIX LAYERS

When there are null points, there are separatrices, and reconnection corresponds to a discontinuous mapping of field lines from one footpoint to another. However, as already discussed, Schindler *et al.*[8] show that in a nonvanishing magnetic field, the field line mappings are continuous and separatrices do not exist. The concept of magnetic flipping describes how reconnection might occur in such a case. In this concept, a volume of field lines passing through a non-ideal region rapidly slip through the plasma, changing their connections along the way. This process first requires a region of large but continuous gradients in the footpoint mapping. A quasi-separatrix layer (QSL) is such a layer of field lines whose footpoints neighbor at one end but map to widely separated locations at the other end. A QSL is a favorable location for magnetic reconnection. If the QSL also supports a parallel electric field, then reconnection occurs for sufficient footpoint motions. In this case, the field line velocity exceeds the local plasma velocity, producing a parallel electric field.[10] The field lines undergo slippage within the layer, as represented in Fig. 1, adapted from Priest and Démoulin.[10] In the QSL depicted here between two planes, footpoint B_2 maps to A_2, and footpoint B_1 maps to A_1. If footpoint B_1 is perturbed towards B_2, its footpoint must shift a large distance, from A_1 to A_2. If the ratio of the speed of the footpoint motion of B_1 to the Alfvèn speed exceeds a certain threshold, then the resulting speed of the footpoint motion of A_1 can greatly exceed the Alfvèn speed, producing a parallel electric field.[9] The field lines then reconnect while rapidly flipping through the diffusion region (here denoted by shading).

The squashing factor Q identifies the footpoints of field lines belonging to the QSL by measuring the gradients of the mapping of footpoints along the layer. Those field lines that are adjacent at one set of footpoints but diverge widely at the other set of footpoints will have a large value of Q.[11] Where one set of footpoints are defined by the positions (x,z) at y_0 and the other by $(X(x,z),Z(x,z))$ at y_1, Q provides a measure of the gradient of the mapping between the two sets as

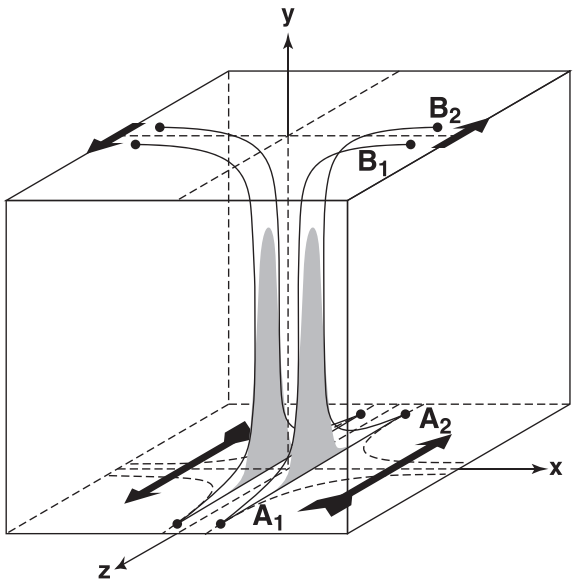

FIG. 1. A schematic portrait of magnetic field lines undergoing reconnection through flipping along a QSL. A small perturbation of point B_1 towards B_2 results in a large displacement of the other footpoint at A_1 towards A_2. If there is a non-ideal electric field, depicted by shading, then the field lines slip rapidly, exceeding the Alfvèn speed, and changing their connections through the layer. The change is, however, topologically continuous, rather than discontinuous. This figure is adapted from Priest and Démoulin.[10]

$$Q = \frac{\left(\frac{\partial X}{\partial x}\right)^2 + \left(\frac{\partial X}{\partial z}\right)^2 + \left(\frac{\partial Z}{\partial x}\right)^2 + \left(\frac{\partial Z}{\partial z}\right)^2}{\left|\frac{B_y(y_0)}{B_y(y_1)}\right|}. \tag{7}$$

Q is normalized by the ratio of the guide field B_y between the two end planes to render the measure insensitive to the choice of end planes.[11] The magnitude of $Q(x,z)$ plotted in the y_0 plane is thus large for those field lines whose endpoints (X,Z) in the y_1 plane have undergone a large displacement as a result of a small displacement in either x or z (and vice versa). Thus, as in Fig. 1, if there is a compression of field lines along x and an expansion along z, for high Q field lines there is a corresponding expansion in Z and compression in X—hence the name "squashing factor."[10]

The QSL consists of those field lines with a high Q, a conservative working definition being Q greater than 10 times the mean value over the volume.[10] Observers, however, have found a maximum Q (non-normalized) of about 4 in solar flares.[21] The exchange along the QSL in which coordinates compress or expand produces a twisted flux tube structure as depicted in Fig. 2. The near end of the tube where field lines converge toward the centerline (shown by arrows) during the flipping process is known as the stable manifold, while the far section of the tube where field lines diverge away from the centerline is the unstable manifold.

This article is copyrighted as indicated in the article. Reuse of AIP content is subject to the terms at: http://scitation.aip.org/termsconditions. Downloaded to IP: 128.154.130.33 On: Mon, 23 Jun 2014 20:00:33

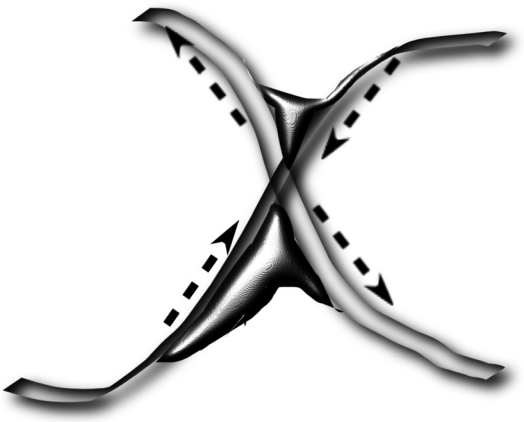

FIG. 2. A front view of the hyperbolic structure of a QSL. The layer is extended along the out-of-page direction and twists from one orientation to another. Here the darker "S" curve lies in the near plane while the lighter curve lies in the far plane. The dashed arrows indicate the direction of motion of field lines that undergo flipping. The section of the layer where field lines move toward the center is the stable manifold while the section where they move away from the center is the unstable manifold.

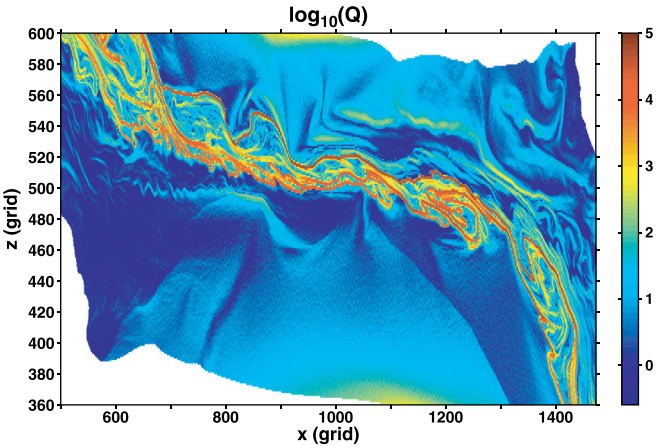

FIG. 3. The log of the squashing factor Q in the $y = 100$ grid point plane of the VPIC simulation for field lines traced to $y = 1024$ grid points. Q is large for field lines that belong to the QSL.

IV. QUASI-SEPARATRIX LAYER IN VPIC

We first derive the squashing factor Q for the inner part of the volume by integrating field lines across $^1/_2$ of the y-domain (i.e., between $y = 100$ and $y = 1024$ grid steps), the direction of the guide field and the initial current layer. Each grid step is $\sim 0.034\ d_i$ based on the Harris reference density, so this corresponds approximately to a span from $y = 3.4\ d_i$ to $y = 35\ d_i$. We limit the integration domain to $^1/_2$ of the y length because the calculations are very computationally expensive and $^1/_2$ of the domain is sufficient for our purposes. While this limitation may omit part of the QSL structure, we find that the integration length is sufficient to achieve a squashing factor ten times the global average, the benchmark we use to define the QSL. The field lines are calculated using both the stream3 function in the Matlab toolbox and, for comparison, by an in-house Python field tracing routine, and both methods show agreement. By numerically differentiating the endpoints of the resulting field lines at $y = 100$ and $y = 1024$, we derive a map of Q in the plane at $y = 100$ for the region $500 < x < 1500$ and $360 < z < 600$. To maximize the computational efficiency, we exclude the outer edges of the x-z plane where the current density is much lower. In our calculation, the denominator in Q is ~ 1 since the guide field is fairly uniform over the volume. Fig. 3 shows the resulting log scale map of Q, where warmer colors signify a larger Q. The white regions correspond to seed points at $y = 100$ whose field lines exit the simulation box before reaching $y = 1024$.

To derive the QSL, we choose those field lines at $y = 100$ whose Q values exceed 10^4, which is just over 10 times the mean value over the domain of seed points at $y = 100$. Fig. 4 depicts the resulting QSL from a view along the y-axis, where the blue surface represents the QSL, and the pink layer at $y = 100$ represents footpoints with $Q \geq 10^4$. The hyperbolic structure of the QSL is evident, as is the exchange of directions of elongation and compression. The QSL defines a likely location for reconnection. To find where reconnection occurs, we must evaluate the integral of the parallel electric field.

V. RECONNECTED MAGNETIC FLUX AND INTEGRATED PARALLEL ELECTRIC FIELDS

A map of Ξ for a fixed y identifies which field lines lie on a gradient in the quasi-potential and therefore are reconnecting. Fig. 5(a) is the resulting map of the quasi-potential Ξ in x-z space in the starting plane at $y = 100$ grid steps after integrating the parallel electric field from $y = 100$ to $y = 1024$ grid steps. The quasi-potential is here expressed in units of $v_A B_0 d_i/c$, where c is the speed of light and $v_A = B_0/(4\pi n_0 m_i)^{1/2}$ is the Alfvèn speed. Figure 5(b) of the current density in the same plane shows a corresponding structure. (Again, the limited range cuts computational costs while producing sufficient information for our purposes. To calculate the reconnection rate, we integrate a subset of field lines all the way through the system, as explained below.) The contours of Ξ collocate with the cross-section of the QSL in the same plane. However, because the theory of general magnetic reconnection is formulated in α-β space, we derive an α-β coordinate system

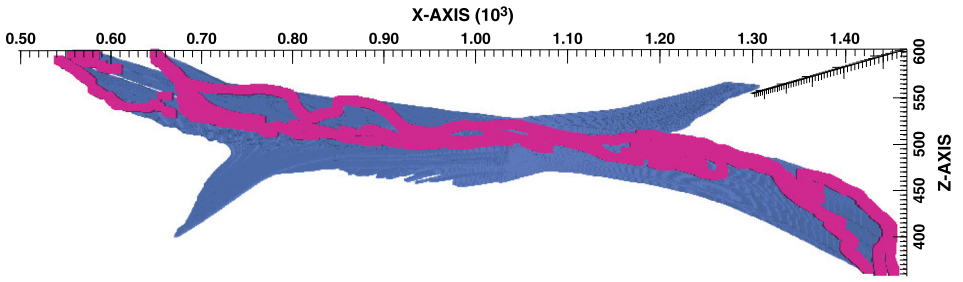

FIG. 4. The hyperbolic structure of the QSL between $y = 100$ and $y = 1024$ grid points based on $Q \geq 10^4$ in the VPIC simulation. The blue surface is the QSL, which twists from one orientation to another along y, and the pink layer corresponds to the endpoints of the QSL at the start plane at $y = 100$.

This article is copyrighted as indicated in the article. Reuse of AIP content is subject to the terms at: http://scitation.aip.org/termsconditions. Downloaded to IP: 128.154.130.33 On: Mon, 23 Jun 2014 20:00:33

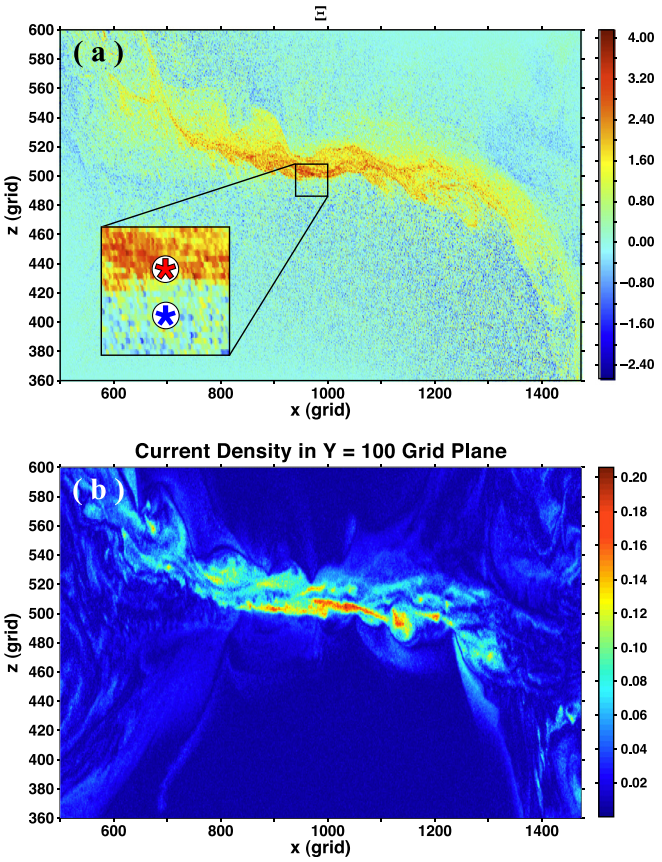

FIG. 5. (a) A map of the quasi-potential Ξ in the $y = 100$ plane, from integration of the parallel electric field between $y = 100$ and $y = 1024$ grid points. The quasi-potential is in units of $v_A B_0 d_i/c$. The two asterisks in the inset denote the footpoints of the two field lines discussed in Figure 9. (b) The magnitude of the current density in the corresponding plane shows a corresponding structure.

in which to create the map. If U(*x*,*y*,*z*) and V(*x*,*y*,*z*) are functions that satisfy

$$\mathbf{B} = F(U,V)\nabla U(x,y,z) \times \nabla V(x,y,z), \tag{8}$$

and $u(x,z)$ and $v(x,z)$ are the values that U and V take on the plane $y = 100$, then in the plane $y = 100$, α and β are functions of u, v, i.e., $\alpha(u,v)$ and $\beta(u,v)$. Because α and β are not unique, we can choose $\alpha = u$ and find the $\beta(u,v)$ that satisfies Eq. (1). Stern[22] shows that

$$\beta(u,v) = \int^{v} f(u,v')dv', \tag{9}$$

where

$$f(u,v) = (B_\perp / [\nabla U_{||} \times \nabla V_{||}]_\perp)_\sigma,$$

and the perpendicular and parallel components refer to the plane σ defined by u and v (here the plane $y = 100$). Here we make the simple choice $U = x + y$ and $V = z + y$, which means $\alpha = u = x$. Then according to Eq. (9)

$$\beta = -\int^{z} B_y(x,z')dz'. \tag{10}$$

There is excellent agreement between the QSL and the boundaries of the region of enhanced Ξ. Fig. 6 shows the

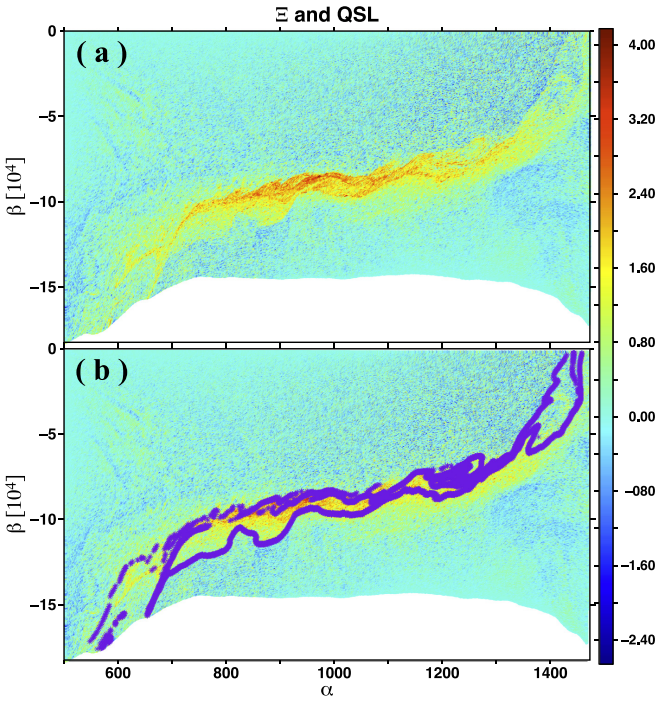

FIG. 6. (a) A map of Ξ in terms of the Euler variables $\alpha = x$ and $\beta = -\int B_y(x,z')\,dz'$. (b) The map of Ξ overlaid with the footpoints of the $Q \geq 10^4$ QSL, shown in purple.

map of Ξ along with the footpoints of the QSL (in purple, Fig. 6(b)) as a function of α and β in the $y = 100$ end plane. Other than an inversion, there is very little change from the mapping in the *x*-*z* plane because of the large guide field. According to the theory of general magnetic reconnection, reconnection occurs where there are gradients in Ξ as a function of α and β. Therefore, it occurs on those field lines that lie on the edges of the area of large Ξ, which also show a high correspondence with field lines that lie on the QSL. General magnetic reconnection also predicts that the gradients in Ξ with respect to α and β occur in closed loops because of the Hamiltonian form of the evolution equations. This prediction also concurs with the shape of the region of large Ξ and the QSL, albeit in a very stretched and elongated shape. The QSL appears to follow the loop-like structure of elevated Ξ and has the appearance of being bifurcated, which in turn correlates with the appearance of a bifurcated current sheet in Fig. 5(b). Therefore, this mapping allows us to identify reconnecting field lines as those field lines on the QSL that correlate with large gradients in Ξ.

VI. DISTRIBUTION OF THE PARALLEL ELECTRIC FIELD ALONG FIELD LINES AND THE RECONNECTION RATE

The question arises as to how the parallel electric field that contributes to the global reconnection rate is distributed along the field lines that support reconnection. In this simulation, $E_{||}$ is highly fluctuating, owing to plasma processes leading to turbulence[13] and, on grid scales, to statistical noise from low particle counts per cell. Figs. 7(a) and 7(b) compare $E_{||}$ along a field line that is reconnecting and one that is not. Following $E_{||}$ along a field line without integrating, it is

This article is copyrighted as indicated in the article. Reuse of AIP content is subject to the terms at: http://scitation.aip.org/termsconditions. Downloaded to IP: 128.154.130.33 On: Mon, 23 Jun 2014 20:00:33

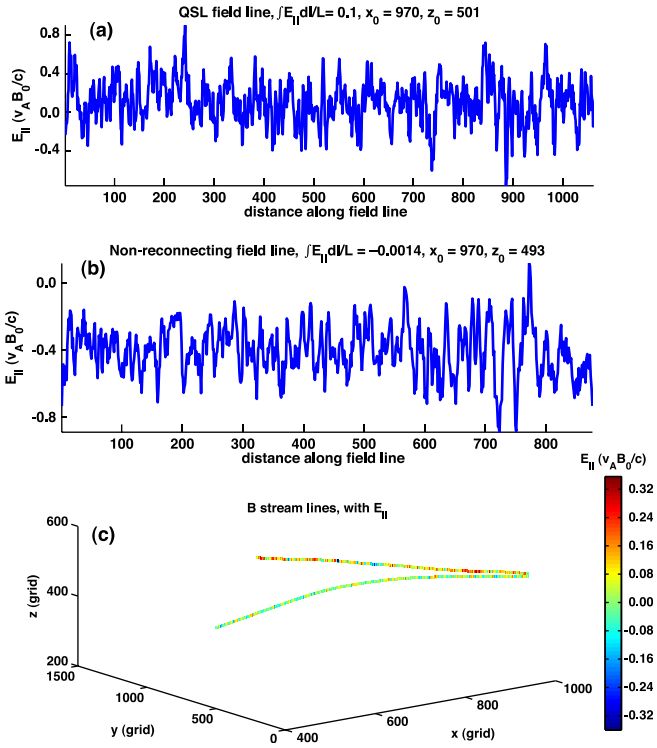

FIG. 7. (a) $E_{||}$ along a reconnecting field line on the QSL. (b) $E_{||}$ along a non-reconnecting field line. (c) The same reconnecting and non-reconnecting field lines colored by $E_{||}$.

difficult to make a judgment where reconnection is occurring, as Fig. 7 attests. Moreover, it is very difficult to distinguish in this way any difference between the reconnecting and non-reconnecting signatures, much less where reconnection might be occurring along the field line. The spatial plot in Fig. 7(c) of the same reconnecting and non-reconnecting field lines that are color-coded according to $E_{||}$ does appear to reveal a higher average $E_{||}$ along the reconnecting field line. Nevertheless, it is not clear to what extent the reconnection is patchy, corresponding to the peaks in the fluctuations, and to what extent the fluctuations contribute to the global reconnection rate. Fig. 8 shows a view along z of the set of QSL field lines colored by $E_{||}$. As Fig. 8 illustrates, some of the fluctuations also organize into Bernstein-Greene-Kruskal (BGK) mode electrostatic solitons, or electron holes.[23,24] The question also arises, therefore, as to what contribution the fluctuations make to the reconnection rate.

For insight to these questions, we calculate the running sum of $E_{||}$ in units of $v_A B_0 d_i/c$ up to each position along the field line and plot this as a function of position along the field line for both reconnecting and non-reconnecting field lines. The footpoint of the chosen reconnecting field line corresponds to the red asterisk in Fig. 5(a) while that of the non-reconnecting field lines corresponds to the blue asterisk in Fig. 5(a). This shows us where reconnection is occurring and how steady it is along the field line. Fig. 9 shows that the sum for the reconnecting field line almost immediately exceeds that of the non-reconnecting line so that we know that the difference does not owe to the fact that the reconnecting field line is longer. Though there are small amplitude fluctuations in the sum and there are some changes in the

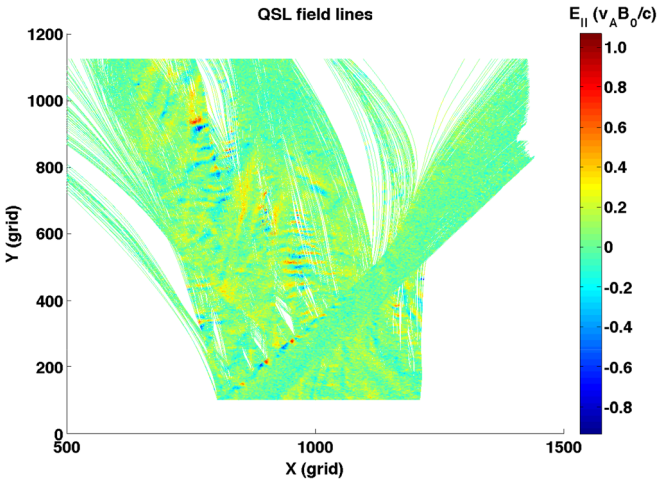

FIG. 8. A view along the -z direction of QSL field lines colored by $E_{||}$, showing fluctuating bands of positive and negative $E_{||}$, like electron holes.

slope, the value is always increasing on average, suggesting that a low-order, rather than highly fluctuating, contribution to $E_{||}$ controls the reconnection rate. To quantify this idea, in Fig. 10 we plot the DC and linear components of $E_{||}$ as a function of field line length for both the reconnecting and non-reconnecting field lines. Though the value of $E_{||}$ decreases with distance along the field line for both types of lines, it is always positive for the reconnecting field line with a much higher average. In fact, the total integral of the DC and linear trend of the reconnecting field line along the full length of the line is almost exactly equal to Ξ, and the integral over just the higher-order fluctuations is vanishingly small. Therefore, the fluctuations, including the electron holes, are not contributing to the global reconnection rate. We note that the electron holes are also observed on non-reconnecting field lines with a negligible parallel electric field. These facts argue against the possibility that a difference in the number of positive and negative layers

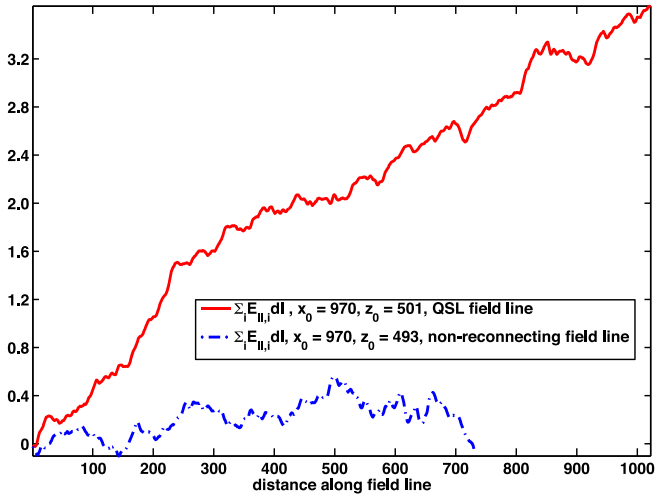

FIG. 9. The running sum of $E_{||}$ (in units of $v_A B_0 d_i/c$) along a reconnecting (solid) and non- reconnecting (dashed) field line as a function of position along the field line smoothes the data. The difference is apparent near the beginning of the field lines, revealing what appears to be a relatively steady contribution to the reconnection rate. Reconnection is occurring anywhere along the field line where the running sum is increasing.

This article is copyrighted as indicated in the article. Reuse of AIP content is subject to the terms at: http://scitation.aip.org/termsconditions. Downloaded to IP: 128.154.130.33 On: Mon, 23 Jun 2014 20:00:33

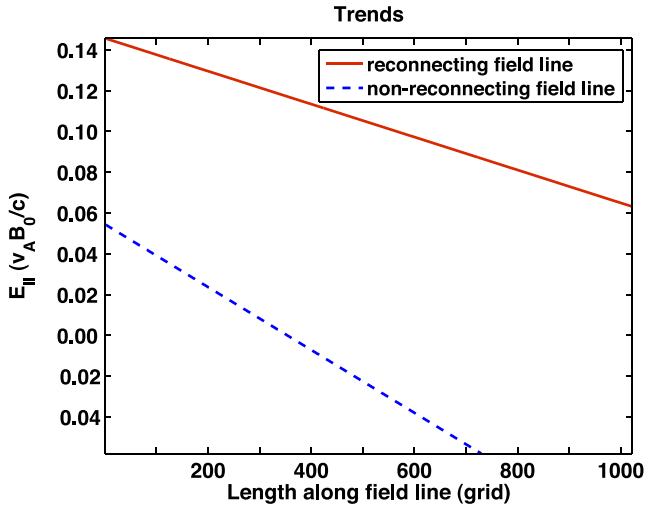

FIG. 10. The parallel electric field filtered to remove all but linear trends in the reconnecting (red) and non-reconnecting (blue) field lines. The reconnecting field line has a non-zero average, and the final reconnection rate owes entirely to the sum over the DC and linear contributions to $E_{||}$ while the fluctuations contribute nothing.

accounts for the growing running sum in Fig. 9. We also observe that the increase in $E_{||}$ along the field line in the direction of the current ($J_y > 0$) is consistent with $J_{||}E_{||} > 0$, or the conversion of magnetic to particle energy.

Finally, we wish to determine the reconnection rate across the flux surfaces of the QSL for the global system. Hesse *et al.*[8] shows that this is given by the maximum value of Ξ along the flux surface in α-β space. From Fig. 6, we discern that this is just over 4, which yields a normalized reconnection rate of about 0.1 when divided by the length of the field line. However, in the event that some information has been lost by dint of the fact that we have only integrated halfway through the system, we integrate a small subset of field lines near the center of the simulation volume all the way from $y = 1$ to $y = 2048$. Fig. 11 shows the result for one of the field lines with a value of Ξ close to the maximum,

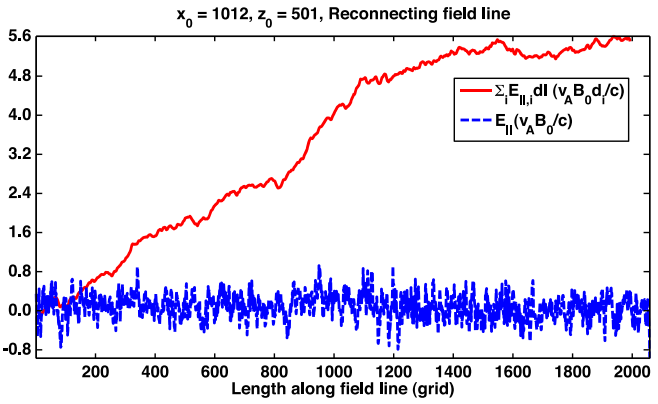

FIG. 11. The running sum of $E_{||}$ in units of $v_A B_0 d_i/c$ (solid line) and the corresponding value of $E_{||}$ in units of $v_A B_0/c$ (dashed line) for a reconnecting QSL field line determined from integrating along the entire length of the system. The peak value of the running sum of $E_{||}$ is about 5.4. When normalized by the length of the nonideal electric field (about 1500 grid cells, or 51 d_i), the normalized reconnection rate is about 0.1 $v_A B_0 d_i/c$, which is about the maximum value anywhere on the QSL. Therefore, this is approximately the reconnection rate across the flux surface of the QSL.

which has a peak value at 1500 grid steps of about 5.4 in units of $v_A B_0 d_i/c$. Beyond this point the sum starts leveling off, signifying reconnection may have decreased or shut off, and that the field line may have reentered an ideal region. Normalizing by this length (about 1500 grid cells, or 51 d_i) gives a normalized reconnection rate of about 0.1 $v_A B_0/c$. The field lines inside the high Ξ region will remain inside the diffusion region for their entire length. However, we expect field lines on the edges of the region to leave the diffusion region at some point. Thus the determination of their potential drop across a nonideal region, from one ideal region to another, follows the prescription of Hesse and Schindler.[7] An estimate of the reconnection rate based on averaging the ion inflow speed U_{iz} and the Alfvèn speed v_A in a region centered on the inflow/outflow region gives a reconnection rate of $\langle U_{iz}/v_A \rangle \sim 0.1$, which provides corroboration of the value derived from Ξ.

VII. SUMMARY AND CONCLUSIONS

We have sought an organizing principle to determine the location and rate of reconnection in a large-scale kinetic simulation of general 3D magnetic reconnection with a guide field and open boundary conditions. The field line evolution appears to be turbulent and the guide field inhibits the formation of null points in the 3D topology, making it challenging to identify where reconnection is happening, though clearly it is. The concept of reconnection through magnetic flipping on a QSL provides a description of how reconnection can occur in this case. We derive the QSL along one-half the length of the system to identify field lines likely to engage in magnetic flipping and find that it consists of a twisted, hyperbolic layer extending through the system. A parallel electric field along the QSL indicates which field lines undergo slippage. Therefore, we create a 2D map of the integrated parallel electric field for each field line. We find that the QSL correlates well with the boundaries of the region of field lines that have a pronounced quasi-potential. This implies that field lines with significant value of the integrated parallel electric field are, in all likelihood, threading current sheets—the natural locations of enhanced Q factors. The QSL carrying a parallel electric field therefore correlates well with the prediction of the theory of general magnetic reconnection that a necessary and sufficient condition for 3D reconnection in the absence of null points is a gradient of the quasi-potential, or integrated parallel electric field, with respect to the Euler variables. The prediction that the reconnection occurs in loop-like structures also agrees with the elongated, but generally loop-like shape of the contours of Ξ. The turbulence produces finer structure within the loop. The maximum Ξ gives a normalized reconnection rate across the QSL of about 0.1 $v_A B_0/c$.

To further illuminate how and where $E_{||}$ is distributed along the QSL field lines that do support reconnection, we follow the partial, or running, sum of the parallel electric field incrementally along the field lines. It is clear that the field lines that are reconnecting carry a relatively steady DC contribution to the reconnection rate that is absent on field lines that are not reconnecting, though both types of field lines

This article is copyrighted as indicated in the article. Reuse of AIP content is subject to the terms at: http://scitation.aip.org/termsconditions. Downloaded to IP: 128.154.130.33 On: Mon, 23 Jun 2014 20:00:33

have fluctuating positive and negative values of the parallel electric field. This conclusion does not necessarily challenge the accepted view that electron-scale, non-ideal processes in a localized region about the reconnecting field line govern reconnection. Rather, the implication is that the observed fluctuations do not account for the underlying parallel electric field that governs the global reconnection rate. However, the temperature anisotropy in the generalized Ohm's law can support a parallel electric field over broader regions not confined to electron scales. When Liu *et al.*[20] investigate the relative importance of temperature anisotropy and electron-scale contributions, such as electron inertia and nongyrotropic pressure, they find that the relative importance of the contributions depends greatly on initial conditions, due to the chaotic nature of the fields. Here we demonstrate that the reconnection rate results entirely from the DC and linear trends in $E_{||}$ and that higher-order fluctuations do not contribute appreciably on the larger scale even though they may have local effects. Moreover, it is clear reconnection is occurring along a field line wherever the running sum of $E_{||}$ is increasing.

The ramification is that the location and rate of reconnection in simulations and observations can be identified with low-order coherent structures even when fields appear turbulent. This conclusion is consistent with the discussion in Leonardis *et al.*[19] While it is certainly possible that the fluctuations contribute to the physics that sustains the average reconnection electric field, it is rather that average, DC field that governs the reconnection rate. The results also impact the inference of reconnection sites and rates in observations, of importance to the upcoming MMS (Magnetospheric Multiscale) mission. Clearly if the medium is not laminar, the global reconnection rate cannot be inferred from a local parallel electric field measurement, but rather must be estimated from the spatial average along a field line or from some other means.

ACKNOWLEDGMENTS

D. E. Wendel would like to thank Vadim Uritsky and John Dorelli for helpful discussions. This research was supported by a NASA Goddard Space Flight Center Science Innovation Fund award and by the MMS Interdisciplinary Science grant to the Goddard Space Flight Center. D. Olson and N. Aunai were supported by the NASA Postdoctoral Program. HK's contributions were supported by AGS grant no. 1104815 and NASA's Heliophysics Theory Program. W.D. was supported by NASA's Heliophysics Theory Program.

Simulations carried out on Kraken were supported by an allocation of advanced computing resources provided by the National Science Foundation at the National Institute for Computational Sciences (http://www.nics.tennessee.edu/).

[1]S. Fukao, M. Ugai, and T. Tsuda, Rep. Ionos. Space Res. Jpn. **29**, 133–139 (1975).
[2]J. M. Greene, J. Geophys. Res. **93**(A8), 8583–8590, doi:10.1029/JA093iA08p08583 (1988).
[3]Y. Lau and J. Finn, Astrophys. J. **350**, 672–691 (1990).
[4]W. I. Axford, in *Magnetic Reconnection in Space and Laboratory Plasmas*, Geophysical Monograph Series Vol. 30, edited by E. W. Hones, Jr. (American Geophysical Union, Washington DC, 1984), pp. 1–8.
[5]B. U. Ö. Sonnerup, in *Magnetic Reconnection in Space and Laboratory Plasmas*, Geophysical Monograph Series Vol. 30, edited by E. W. Hones, Jr. (American Geophysical Union, Washington DC, 1984), pp. 92–103.
[6]V. M. Vasyliunas, Rev. Geophys. Space Phys. **13**(1), 303–336, doi:10.1029/RG013i001p00303 (1975).
[7]M. Hesse and K. Schindler, J. Geophys. Res. **93**(A6), 5559–5567, doi:10.1029/JA093iA06p05559 (1988).
[8]M. Hesse, T. G. Forbes, and J. Birn, Astrophys. J. **631**, 1227–1238 (2005).
[9]K. Schindler, M. Hesse, and J. Birn, J. Geophys. Res. **93**(A6), 5547–5557, doi:10.1029/JA093iA06p05547 (1988).
[10]E. R. Priest and P. Démoulin, J. Geophys. Res. **100**(A12), 23443–23463, doi:10.1029/95JA02740 (1995).
[11]V. S. Titov, G. Hornig, and P. Démoulin, J. Geophys. Res. **107**(A8), 1164, doi:10.1029/2001JA000278 (2002).
[12]H. Che, J. F. Drake, and M. Swisdak, Nature **474**, 184–187 (2011).
[13]W. Daughton, V. Roytershteyn, H. Karimabadi, L. Yin, B. J. Albright, B. Bergen, and K. J. Bowers, Nat. Phys. **7**, 539–542 (2011).
[14]J. F. Drake, M. Swisdak, C. Cattell, M. A. Shay, B. N. Rogers, and A. Zeiler, Science **299**, 873–877 (2003).
[15]H. Karimabadi, V. Roytershteyn, M. Wan, W. H. Matthaeus, W. Daughton, P. Wu, M. Shay, B. Loring, J. Borovsky, E. Leonardis, S. C. Chapman, and T. K. M. Nakamura, Phys. Plasmas **20**, 012303 (2013).
[16]W. Daughton, J. Scudder, and H. Karimabadi, Phys. Plasmas **13**, 072101 (2006).
[17]K. J. Bowers, B. J. Albright, L. Yin, B. Bergen, and T. J. T. Kwan, Phys. Plasmas **15**, 055703 (2008).
[18]K. Bowers *et al.*, J. Phys.: Conf. Series **180**, 012055 (2009).
[19]E. Leonardis, S. C. Chapman, W. Daughton, V. Roytershteyn, and H. Karimabadi, Phys. Rev. Lett. **110**, 205002 (2013).
[20]Y.-H. Liu, W. Daughton, H. Karimabadi, H. Li, and V. Roytershteyn, Phys. Rev. Lett. **110**, 265004 (2013).
[21]P. Démoulin, L. van Driel-Gesztelyi, B. Schmieder, J. C. Hénoux, G. Csepura, and M. J. Hagyard, Astron. Astrophys. **271**, 292–307 (1993).
[22]D. P. Stern, Am. J. Phys. **38**(4), 494–501 (1970).
[23]M. V. Goldman, F. Carey, D. L. Newman, and M. Oppenheim, Phys. Plasmas **7**, 1732 (2000).
[24]M. V. Goldman, D. L. Newman, and P. Pritchett, Geophys. Res. Lett. **35**, L22109, doi:10.1029/2008GL035608 (2008).

This article is copyrighted as indicated in the article. Reuse of AIP content is subject to the terms at: http://scitation.aip.org/termsconditions. Downloaded to IP: 128.154.130.33 On: Mon, 23 Jun 2014 20:00:33